Int J Adv Manuf Technol (2011) 57:969–982
DOI 10.1007/s00170-011-3355-x

ORIGINAL ARTICLE

A step towards the in-process monitoring for electrochemical microdrilling

M. A. H. Mithu · G. Fantoni · J. Ciampi

Received: 21 January 2011 / Accepted: 17 April 2011 / Published online: 15 May 2011

Abstract The electrochemical micromachining appears to be a promising candidate as a future micromachining technique that utilizes high frequency pulses for micron- to nanoscale material dissolution. This article presents a step towards the in-process monitoring based on waveforms generated during electrochemical micromachining. An attempt has been taken to correlate between the waveforms generated during machining and experimental outcomes such as material removal rate, machining time, and the dimensions of the microholes fabricated on commercially available nickel plate with prefabricated tungsten microtools. An electrical function generator is used as a signal source and a digital storage oscilloscope is provided for observing the nature of electrical pulses used and recording the waveforms generated during machining. The waveforms are subgrouped depending on the parameters used and analyzed to correlate the waveform shape and the machining outcomes. The digital storage oscilloscope also facilitates for observing the short-circuit condition which may occur during microdrilling. These results show that the shape of the waveforms and their corresponding values are in good agreement with the material removal rate, machining time, and on the dimension of fabricated microholes. Therefore, the proposed monitoring technique can be employed as a predictive tool in electrochemical micromachining.

Keywords Electrochemical microdrilling · In-process monitoring · Material removal rate · Microtool · Microhole

M. A. H. Mithu (✉) · G. Fantoni · J. Ciampi
Department of Mechanical, Nuclear and Production Engineering,
University of Pisa,
56126 Pisa (PI), Italy
e-mail: ah.mithu@ing.unipi.it

G. Fantoni
e-mail: g.fantoni@ing.unipi.it

1 Introduction

The up-and-coming global trend toward the miniaturization of manufacturing processes are clearly driving developments in microscale processes to meet needs related to miniaturized parts and products, accuracy and precision, and materials developments. With the development of micromanufacturing technologies, various microparts and micromachining methods are becoming important [1]. However, such precision microparts cannot be realized using traditional machining processes [2]. Therefore, for fabricating these microproducts, several conventional and nonconventional processes have been developed. The electrochemical micromachining (μECM) is one of the promising candidates among them [3]. This process engrosses selective metal dissolution from unprotected surfaces of an electrically conductive workpiece that is made an anode in the electrolytic cell. Dissolution of anode is performed in electrolytes when a DC and/or pulsed DC current is applied between the electrodes. The workpiece and/or the electrode tool must be moved relatively to each other in order to maintain a predefined gap, and electrolyte flows between the electrodes within the gap. This process does not need any contact between tool and workpiece, and neither a thermal or mechanical stress on the workpiece material nor a heat-affected zone is generated offering a nice quality machined surface. Therefore, μECM finds many applications in microhole drilling and micromilling, in 3-D micro-shaping, deburring, etc. [4, 5].

The μECM is, therefore, a facile technique for the topographical dissolution of conductive materials through control of current density or applied voltage, etching time, electrolytic flow and its composition, concentration, etc. [6, 7]. In the last decade, the application of short voltage pulses

in mask-free electrochemical micromachining has been studied by different researchers [8–11]. The use of short pulses is proven to be an absolutely necessary technology for the localized material dissolution process. In pulsed electrochemical machining, the useful values of the on- and off-pulse times are limited by the rate of charging and discharging, respectively, of the electrical double layer, which is defined as the structure of charged ions or oriented dipoles that always forms at the interface of an electrode when it is immersed into an electrolyte solution [12]. On the application of a potential difference between two electrodes, the potential profile in the electrical double layer becomes similar to that of an equivalent circuit of capacitors and resistors [6]. However, all the current flow through an electrochemical cell is not caused by electrochemical reactions. There is reaction current called faradaic current and transient current called non-faradaic current [13]. Faradaic current determines the material dissolution rate and non-faradaic current results from current flow that charges and discharges only the double layer capacitance [14]. Beside the controlling parameters, the dimension of microtool also determines the material removal rate of μECM [14, 15].

Inter-electrode gap is also a key factor deciding precision, machining efficiency, and surface quality of workpiece in μECM [16]. As there is no limitation of machining shape, the shape and size of the microtools becoming smaller and with various end shapes [17], complexity is increasing for these microtools in the μECM [18]. Hence, monitoring and controlling the interelectrode gap is very difficult [16]. While the growths in the functionability of highly sophisticated electrical and electronic components offer the opportunity to improve the level of process monitoring and control, there still have not any effective methods that can be used to on-line process monitoring and control [19, 20]. Moreover, the costs of these equipments are very high.

On the other hand, a typical μECM is electrically and chemically noisy. Most of the μECM researches are carried out into toxic electrolytes like HCl, H_2SO_4, HF, $HClO_4$, HNO_3, and their mixtures. The use of toxic electrolyte in μECM has been an obstacle for the widespread of micro-electrochemical fabrication technology [10]. Moreover, the etching process produces H_2 gas, can form bubbles that can prevent the movement of fresh etchant to the surface, and the gaseous H_2 can cause airborne fumes may result in irritation and sensitization of the lungs or other mucous membranes [21]. In addition, the tool electrode advanced towards the workpiece at a constant feed rate where the dissolution takes place into a very tiny space. Thus, the formation of bubbles around the diffusion layer makes the sighting problems [22]. But, if material removal rate cannot keep pace with the feed rate, the microtool touches the workpiece and cause short circuiting. The result is highly detrimental for μECM because of extensive damage of workpiece and/or damage of the microtool tip [23].

From the aforementioned literatures, it emerges that: (1) μECM is one of the promising candidates for fabricating microparts, where the machining accuracy increases when the pulse voltages are applied with appropriate duty ratio, (2) besides the controlling parameters, the microtool determines the geometry of machined part, and (3) μECM process demands an in-processes monitoring and control system that reduces the detrimental effects associated to μECM processes. This article is, therefore, devoted to develop an in-process monitoring system based on results found from a digital data storage oscilloscope during microdrilling on a nickel plate. Three electronic components, namely, a function generator, an oscilloscope and a tailored circuit are used for this purpose. The material removal rate (MRR), machining time, and the dimensions of fabricated microholes are considered as response factors and compared to the waveforms generated during machining.

2 Experimental procedure

2.1 Experimental setup

The self-developed electrochemical micromachining workcell is shown in Fig. 1. It consists of an electrical function generator, an oscilloscope, computer controlled guide system for feeding the tool and the workpiece. The guides were controlled by a 3-axes microstep controller system that was interfaced with a desktop computer. The controller was controlled by customized software. The specifications of the testing equipments are given in Table 1. To avoid the physical contact between the tool (tungsten) and the workpiece (nickel plate), a tailored electronic circuit was used that automatically stopped and retracted the tool. After the set time, the circuit automatically restarted feeding the tool maintaining the predefined gap between the workpiece and tool. Moreover, the function generator, the oscilloscope, and the tailored circuit were used as signal source, signal analyzer, and tool feed controller, respectively, for in-process monitoring and controlling systems. Experiments were performed at room temperature. As the slender electrode was used, it was very difficult to pump electrolyte throughout the machining area because of its tendency to bend on the application of forced flow of electrolyte. Therefore, no circulation system was integrated during experimentation as μECM process involved negligible heat generation and the amount of precipitation was very small [24].

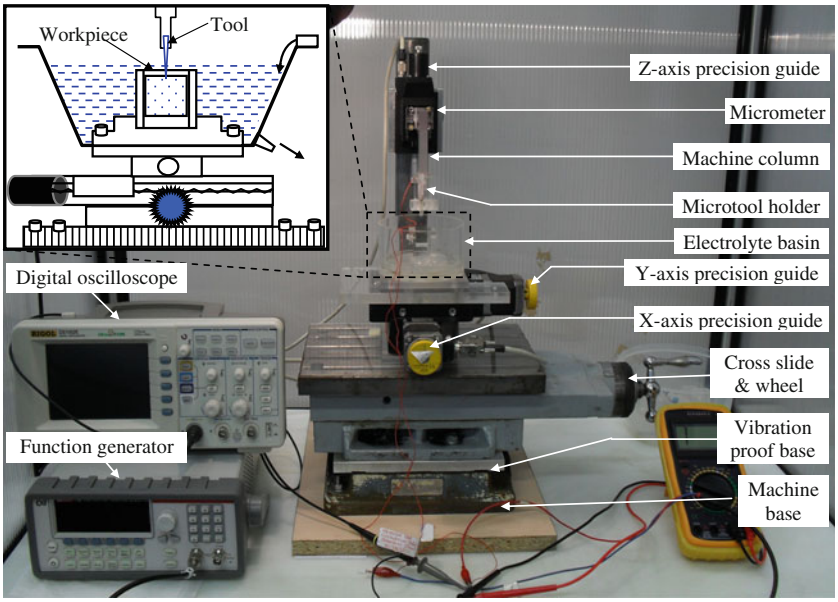

Fig. 1 Electrochemical micro-machining workcell

2.2 Principle of material removal with pulsed voltage

The amount of material removed during μECM can be determined by combining Faraday's first law and Ohm's law as stated in Eq. 1.

$$V_m = \frac{\mathrm{CEA}}{\mathrm{gr}} t \tag{1}$$

where, V_m=volume of material removed, C=the electrochemical constant, E=voltage value acquired by oscilloscope, A=electrode area, g=inter-electrode (tool–work) gap, r=electrolyte resistivity, t=time allowed for machining. This equation is derived assuming 100% efficiency. But for pulsed μECM, the volume of material removed for each voltage pulse is based on the assumption that material is removed only during the fraction of pulse on-time where faradaic current takes place and flow rate is adequate to flush away the reaction products. Since the charging and discharging time depend on the constant resistor–capacitor circuit, material removal generally occurs in areas where electrolyte resistance is lower, i.e., where the tool–work-piece gap is very small. During every pulse period, the double layer is charged and discharged (i.e., created and destroyed) periodically over the two electrodes. The charging and discharging waveform attained during machining is shown in Fig. 2. As, it is not simple to determine the faradaic current duration and its initial time, t^* (Fig. 2), a mathematical model has been proposed to calculate the material removal rate during the pulse on-time with a good approximation [15].

Considering that in the etching process, material removal takes place only for all pulse-on time durations; the volume of material removed (V_m) could be obtained as:

$$V_m = \int_0^{\tau_{on}} \frac{\mathrm{CEA}}{\mathrm{gr}} \mathrm{dt} \tag{2}$$

where, τ_{on} is pulse-on time during each pulsed period.

Since the material removal occurs only during the time corresponding to faradaic currents, the integral has to be rearranged accordingly for better approximation as follows:

Table 1 Specifications of testing equipments used for electrochemical machining workcell

Test equipment	Specifications
Function generator	Keithley 3390 50 MHz; frequency resolution, 1 μHz; amplitude, 10 mV_{pp}–10V_{pp}; 4 digits resolution; phase range, –360° to +360°; accuracy, 8 ns
Oscilloscope	Rigol DS1000E, 1 GHz, 2 channel, digital storage, 64 K color display
Linear travel guide	PLS-85, X and Y axes, maximum travel 155 mm, resolution 0.1 μm, uni-directional repeatability 0.05 μm, maximum 100 mm/s, and ML 40, Z-axis, maximum travel 40 mm, resolution of 0.1 μm, maximum 5 mm/s
Microcontroller	SMC corvus eco, 3-axes closed loop control, velocity <0.1 μm/s, 15–25 rev/s, linear interpolation, miCos GmbH

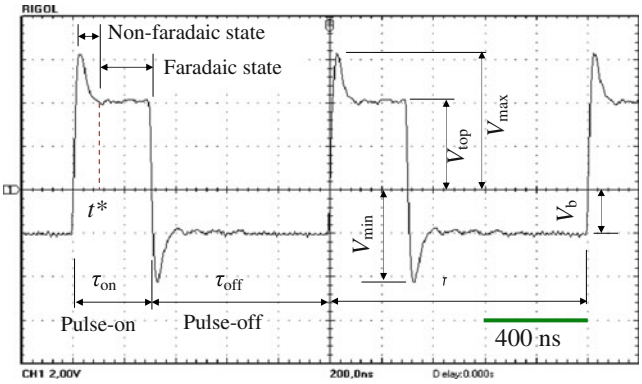

Fig. 2 Charging and discharging waveform formed during machining

$$V_{\text{on-time}} = \int_{t^*}^{\tau_{on}} \frac{\text{CEA}}{\text{gr}}\text{dt} = \int_{t^*}^{\tau_{\text{on}}} \left[\int_s \frac{\text{CA}}{\text{gr}}\text{Eds}\right]\text{dt} \tag{3}$$

$$= \text{CE}^* \int_{t^*}^{\tau_{on}} \left(\frac{\text{S}'}{\text{g}'\text{r}'}\right)\text{dt}$$

$$V_{\text{on-time}} = \frac{\text{CS}'E^*}{g'.r'}\left(\tau_{\text{on}} - t^*\right)$$

where, S is the surface immersed into electrolyte, t^* is the start time of the flat voltage, and E^* is the flat voltage from t^* to τ_{on}, and S', g', r' are the average values of S, g, and r, respectively, coming from the surface integral. The values of g and r vary along the surface and have a minimum value in the closer part of the tip that supplies the higher contribution to the surface integral.

Again, τ_p is the time taken for one complete oscillation and δ_τ is the fraction of τ_p, called duty cycle in percentage, and γ^* is the percentage of pulse-on time to start almost-flat voltage (median value of E becomes almost-flat voltage) and is measured with the aid of a digital oscilloscope. Putting these in Eq. 3,

$$V_{\text{on-time}} = \frac{\text{CS}'\text{E}^*}{\text{g}'\,\text{r}'}\delta_\tau\left(1-\gamma^*\right)\tau_p = \frac{\text{CS}'\text{E}^*}{\text{g}'\text{r}'\text{f}}\delta_\tau\left(1-\gamma^*\right) \tag{4}$$

where, f is the applied frequency in hertz (cycles per second). However, this approximation by excess of MRR was calculated as

$$\text{MRR} \cong \frac{V_{\text{on-time}}}{\tau_{\text{on}} + \tau_{\text{off}}} = \frac{V_{\text{on-time}}}{\tau_p} \tag{5}$$

where, $V_{\text{on-time}}$ is the volume of material removed for one pulse on-time.

2.3 Fabrication of microholes

Tungsten and its alloys are widely used as tool material because of its high electric and thermal conductivity, corrosion resistance, stiffness to withstand the pressure of electrolyte, and mechanical strength. In this experiment, straight tungsten wire of 0.38 mm in diameter was used to fabricate microtools. The required tungsten piece was cut from the supplied long wire and the ends of the specimen were ground, polished, and cleaned. Tools were fabricated by reversed electrochemical process where the tungsten specimens were considered as workpiece. The specimens were fixed to a holder unit and immersed vertically at a constant depth into the electrolytes basin containing caustic solution of 0.1–1.4 M concentration. On the application of a potential difference between electrodes, the dissolution process proceeded and a certain etching time resulted in a straight microshaft with a certain diameter. Each of the tools was rinsed in the hot water to remove foreign particles and formed oxides.

Besides, an uncoated nickel plate of 50×50×0.075 mm in dimension was selected as work material. Less toxic and dilute electrolyte, 0.2 M HCl was selected during microholes fabrication. Hence, the acidic electrolyte allowed refreshing electrolyte in the machining area easily, because the acid electrolyte usually produced by-product much less than common salt electrolytes. The prefabricated microtools shank part were covered with plastic shield and fixed with the holder unit, positioned vertically downward, and fed towards the nickel workpiece. At the initial time of machining, the interelectrode gap was kept in the range of 10–12 μm [23, 24], and microtool feeding was controlled by the servo-controlled feed mechanism of ML 40, Z-axis travel guide, while the workpiece was positioned horizontally by X–Y axes travel guides, if required. The machining conditions applied in microdrilling process are summarized in Table 2.

Image analysis application software, Easy Analysis, integrated to the optical microscope (Nikon SMZ800) was used to measure the diameter and length of the tool produced by μECM. Entrance and exit diameters of each fabricated microhole were also measured using the same microscope. In addition, scanning electron microscope was used to acquire clear picture of the fabricated microtools and microholes.

However, the entrance and exit diameter of the machined microhole were not same due to corner etch of the hole entrance in addition with the linear etching and the result was the tapering of the side wall. Therefore, to evaluate the total material removed during machining, both entrance and exit diameters were measured. Referring to Fig. 3, the amount of material removed during machining was calculated from the truncated cone equation:

$$V_m = \frac{\pi h}{12}\left(\phi_{\text{ent}}^2 + \phi_{\text{ent}}.\phi_{\text{exit}} + \phi_{\text{exit}}^2\right) \tag{6}$$

where $\varnothing_{\text{ent}}$, $\varnothing_{\text{exit}}$, h, g_{ent}, g_{exit}, and $\varnothing_{\text{t}}$ were hole entrance diameter, hole exit diameter, thickness of the metal plate, entrance side gap, exit side gap of the microhole, and microtool diameter, respectively. The actual material

Table 2 Machining conditions for microhole fabrication

Factors	Parameters/value
Working materials	Tool: tungsten 0.38 mm (Goolfellow Ltd, UK)
	Work: nickel plate, 50×50×0.075 mm (Goodfellow Ltd, UK)
Electrolyte concentrations (M/L)	Tool fabrication: 0.1–1.4 M KOH
	Microdrilling: 0.2 M HCl solution
Electrical parameters	Applied frequency: 0.5–2 MHz
	Duty cycle: 15–40%
	V_{pp}: 16.1 V
	V_{max}: 10.6 V
	V_b: −5.0 V
Tool feed	0.05–0.8 μm/s, computer controlled

removal rate (MRR_{act}) was calculated as the total volume of material removed from the workpiece divided by the required total machining time, and expressed as cube millimeter per minute. Input variables for each experiment and corresponding experimental results are summarized in Table 3.

3 Experimental results and discussion

To establish the in-process monitoring system, the shapes of the waveforms that formed during microdrilling on nickel plate were captured, and stored. These stored waveforms were subgrouped into different categories: (1) waveforms for different tool diameters, (2) waveforms for various tool lengths, (3) waveforms for different applied potentials, (4) waveforms for different applied frequencies, and (5) waveforms for different duty cycles, to see how the shape of the waveform and different values of the corresponding waveshape influenced on the MRR, and also on the microproduct's quality. In pulsed electrochemical process, the current resulting from a change in oxidation state of the electroactive species is termed the faradaic current because it obeys Faraday's law. The exact shape and magnitude of the potential profile represents the amount of faradaic and non-faradaic current generated that practically governed material dissolution process. As the faradaic effect, the product of voltage value acquired by oscilloscope ($E^* = V_{top}$) and the time for remaining the voltage value at this level, determined how much material was dissolved for a single pulse, the total faradaic effect was calculated from the product of faradaic current and the total time required for that particular machining, determined the total amount of material dissolved during machining.

3.1 Effect of tool diameter on the waveform

To investigate the relationship between the microtool diameter and the waveform shape, only the microtool diameters were varied and the other parameters were kept constant. Three cylindrical microtools of 21, 41, and 74 μm diameters with the same length were employed for this experiment. During machining, different waveforms were observed, are illustrated in Fig. 4. From the figure, it is observed that the amount of faradaic effect ($V_{top} \times t_{faradaic}$) increases with the increase in the microtool diameter.

This observation can be explained in accordance with the Eqs. 2 to 4, where the selected applied frequency is 1 MHz and pulse-on time is fixed to 300 ns (30% duty cycle) which is much higher than the required ultrashort voltage pulses [14]. Therefore, effect of nontransient current becomes negligible and faradaic current dominates the material dissolution process. From the figure, the voltage values acquired by oscilloscope (V_{top}) and the time for remaining for faradaic current both increase with the increase in microtool diameter. Therefore, the total faradaic effect is amplifying, and the result is that the MRR increases rapidly with the microtool diameter as illustrated in Fig. 5. This is due to the fact, as the surface of electrode area increases, the electrical double layer capacitance increases and electrolytic resistance decreases. The decreased electrolytic resistance increases the current density into the electrolyte. Therefore, the amount of faradaic effect increases with the increase in the current

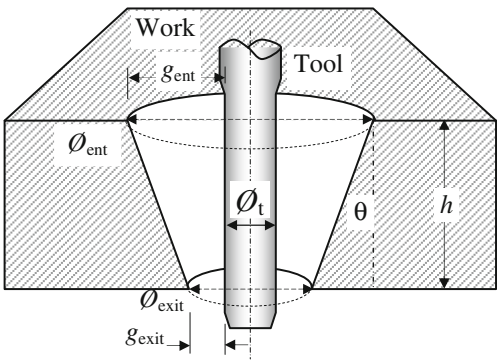

Fig. 3 Schematic illustration of the fabricated microhole

Table 3 Input variables for each experiment and corresponding experimental results

Main Parameters	Electrolyte temperature	Machining time (min)	Tool feed (μm/s)	Number of short circuits	MRR (mm^3/s)	Hole diameter (μm)	
						$Ø_{ent}$	$Ø_{exit}$
Microtool diameter effect: (for f=1 MHz, pulse time, τ=1.0 μs, duty cycle, δ_τ=30%, 0.2 M HCl)							
$Ø_{tool}$=21 μm	Room temperature	6.5	0.3	0	3.48×10^{-7}	54	42
$Ø_{tool}$=41 μm		20	0.1–0.15	1	5.57×10^{-7}	112	101
$Ø_{tool}$=74 μm		30	0.1	1	9.40×10^{-7}	174	165
Microtool length effect: (for f=1 MHz, pulse time, τ=1.0 μs, duty cycle, δ_τ=30%, 0.2 M HCl)							
L=600	Room temperature	17	0.1–0.2	0	16.3×10^{-7}	177	159
L=1370		20	0.1–0.15	1	5.57×10^{-7}	112	101
L=3725		50	0.05–0.1	4	1.33×10^{-7}	92	72
Applied potential effect: (for f=1 MHz, pulse time, τ=1.0 μs, duty cycle, δ_τ=30%, 0.2 M HCl)							
V_{pp}=4.6 V	Room temperature	80	0.05	15	0.83×10^{-7}	92	71
V_{pp}=8.4 V		23	0.05–0.1	1	5.14×10^{-7}	122	97
V_{pp}=17.2 V		20	0.2–0.4	0	9.62×10^{-7}	141	139
Applied frequency effect: (for $Ø_{tool}$=76 μm, L=690 μm, duty cycle, δ_τ=30%, 0.2 M HCl)							
f=0.5 MHz	Room temperature	12	0.2–0.8	0	6.01×10^{-6}	276	266
f=1.0 MHz		16	0.2–0.4	1	2.24×10^{-6}	192	190
f=1.5 MHz		18.5	0.2	1	1.85×10^{-6}	190	183
f=2.0 MHz		23.5	0.1	1	1.20×10^{-6}	174	165
Duty cycle effect: (for $Ø_{tool}$=76 μm, L=690 μm, f=1.0 MHz, 0.2 M HCl)							
δ_τ=15%	Room temperature	116	0.05	25	0.095×10^{-6}	112	110
δ_τ=25%		35	0.1	3	0.811×10^{-6}	174	166
δ_τ=30%		20	0.2	1	1.39×10^{-6}	177	159
δ_τ=35%		10	0.3	0	5.80×10^{-6}	247	239
δ_τ=40%		6	0.4	0	11.84×10^{-6}	273	264

density into the electrolyte, and causes rapid increase in material dissolution rate.

From Fig. 5, it also reveals that the machining time increases with an increase in the diameter. With the increasing machining time, the side gap ratio, the ratio of the gap at the entrance (g_{ent}) to the gap at the exit (g_{exit}) of the fabricated microhole, decreases, as it is found to be related with the machining time. The entrance and exit diameter of the fabricated microhole are shown in the same figure.

3.2 Effect of tool length on the waveform

Three microtools, such as short tool (smaller than 1.0 mm, i.e., $L\leq1.0$ mm), medium tool ($1.0<L\leq3.0$ mm), and long tool ($3.0\text{ mm}<L$), respectively, with the same mean diameter were employed for this experiment, and the other parameters were kept constant. Figure 6 shows the effects of overall tool length on waveform generated during machining. From the figure, it is evident that the faradaic effect decreases with the increase in the tool length.

Figure 6 exhibits that the voltage value acquired by V_{top}, and time of that voltage value at this level, ($t_{faradaic}=\tau_{on}-t^*$) both are decreasing with the increase of tool length, and the result is the gradual decrease in the faradaic effect. The decreased faradaic effect decreases the MRR, and increases machining time. Therefore, it is clear that MRR_{act} decreases and the machining time increases with the increase in tool length, as illustrated in Fig. 7.

This observation can be explained in accordance with the Ohm's law as stated in the article published elsewhere [15]. Because of the shorter tool, short path resistance R_s is smaller than the long path resistance R_l and the double layer charging time constant τ_s of the shorter path is relatively

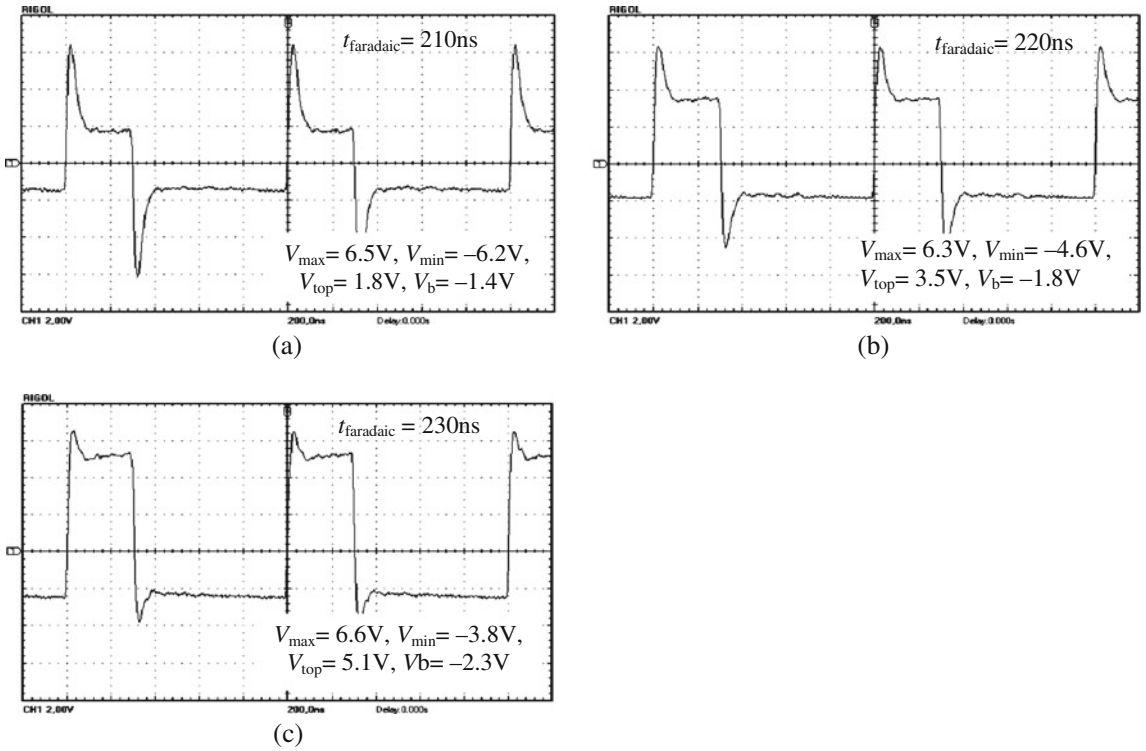

Fig. 4 Waveforms generated during machining for a microtool of **a** 21 μm, **b** 41 μm, and **c** 74 μm in diameter

small compared to charging time constant of long path τ_l. Therefore, faradaic effect decreases with the increase in tool length, as a consequence of this reduction in faradaic effect, the material removal rate decreases proportionately to the rate of increase in electrolyte resistance. Moreover, for a short tool length, the machinable area is restricted to the adjacent region of the tool as the electric current flows through the shorter path with the electrolyte resistance R_s. As a result, the diameters of the fabricated microholes are found to be small for long microtool and vice versa. The diameters of fabricated microholes are also shown in Fig. 7.

3.3 Effect of applied potential on the waveform

Experiments were conducted with pulse amplitude in range of 4.6–17.2 V and pulse duration of 1 μs. In spite of the transpassive dissolution region, electrochemical dissolution did not occurred under 4.0 V. The experiment was,

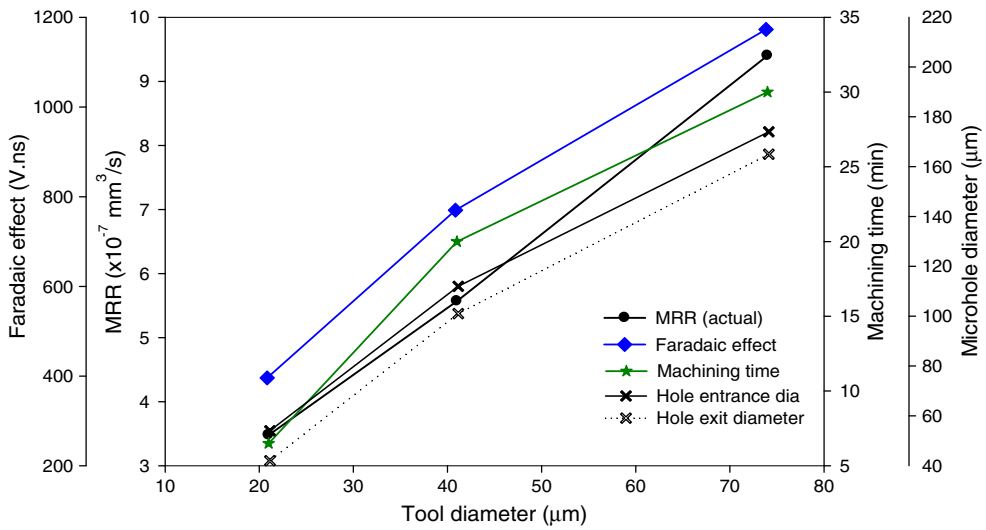

Fig. 5 Effect of tool diameter on faradaic effect, MRR, machining time, and the fabricated microholes

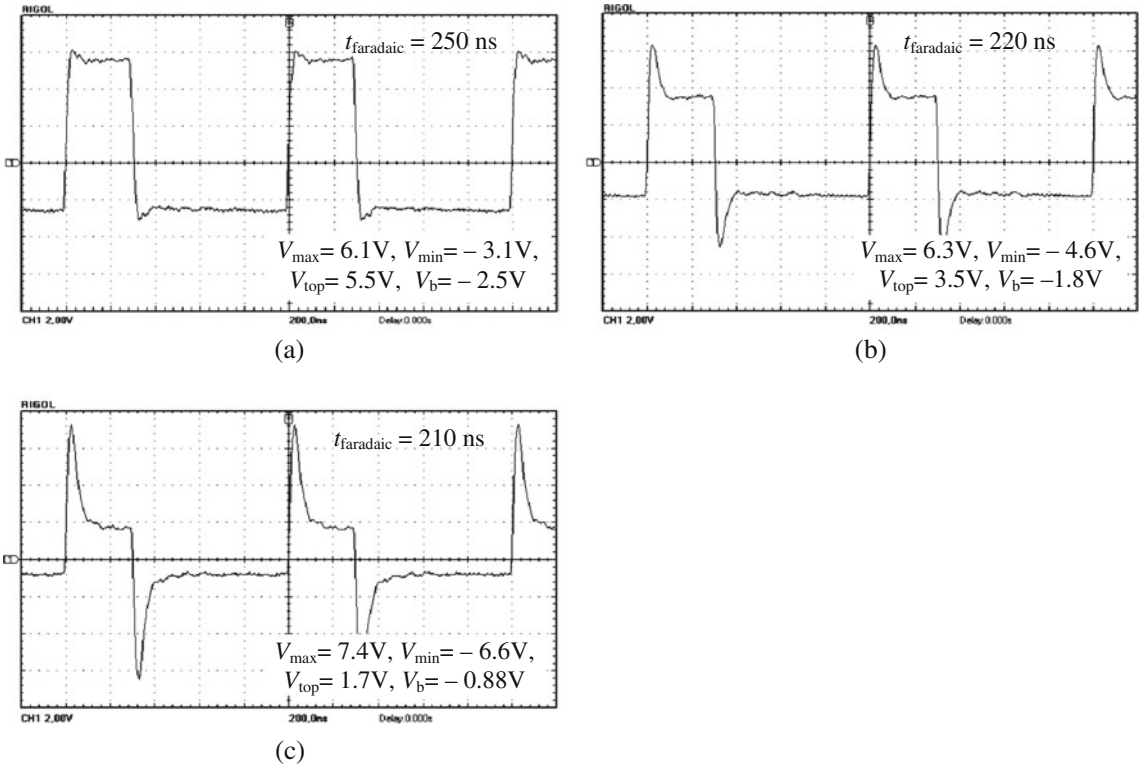

Fig. 6 Waveforms generated during machining for **a** short, **b** medium, and **c** long microtools

therefore, started from 4.6 V. Three different values of peak-to-peak voltage (V_{pp}) were employed to drill on the nickel plate. Figure 8 shows the influence of peak-to-peak voltage on the faradaic effect, machining time, actual material removal rate (MRR_{act}) and the dimensions of micro drilled holes. With increasing applied potential, the amount of faradaic effect, the MRR and diameter of microholes increased, whereas the machining time and the side gap ratio expectedly decreased. When the applied potential was low (V_{pp}=4.6 V), the number of short circuit was found to be very high (15 times) at a moderate feed rate of 0.05 μm/s and total time required for making a single hole was around 80 min which was not feasible in practice. However, when the applied potential was made double, it was possible to increase the feed rate three times leading to reduction of the total machining time by more than 60% and a few short circuits. Though reduction in total machining time was insignificant, no short circuit was observed for the same feed when the applied was increased to 17.2 V. The waveform shown in Fig. 9 demonstrate that

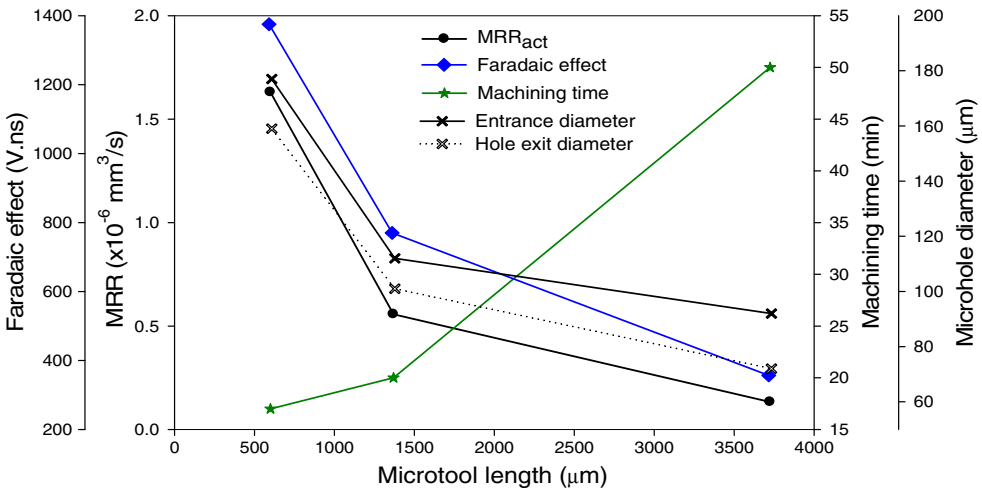

Fig. 7 Effect of tool length on faradaic effect, MRR_{act}, machining time, and the fabricated microholes

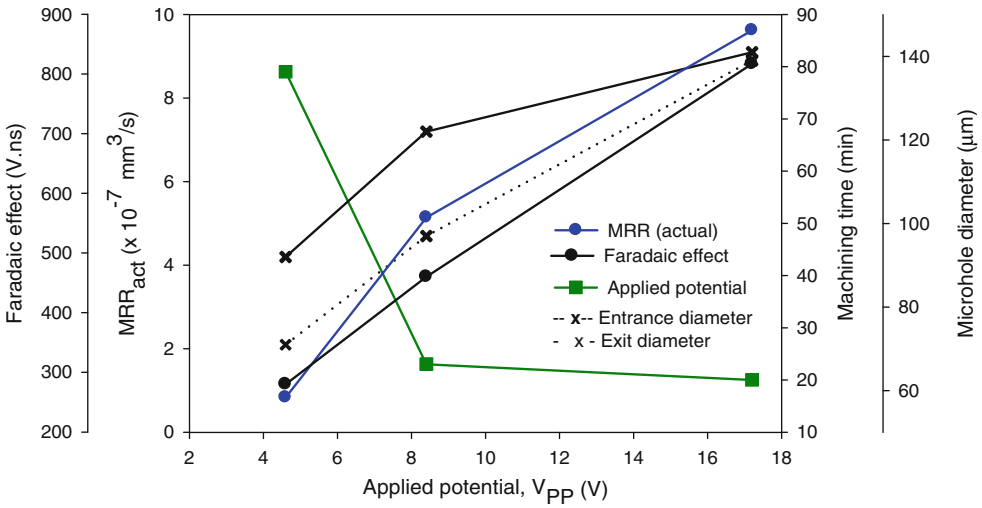

Fig. 8 Effect of applied potential on faradaic effect, MRR, machining time, and the fabricated microholes for f=1 MHz, pulse time, τ=1.0 μs, duty cycle, δ_τ=30%, 0.2 M HCl electrolytes

the amount of faradaic effect was very low for lower applied potentials and reached to a considerable range for higher applied potentials. Therefore, any increase in the applied voltage, i.e., the increased peak-to-peak voltage increased the machining rate that was calculated from the microhole diameters. The entrance and exit diameter of the fabricated microholes are shown in Fig. 8.

From Fig. 9, the voltage values acquired by V_{top} and the time for remaining for faradaic current both increase with the increase in applied potential. Therefore, the faradaic effect is amplifying and the result is that the MRR increases rapidly with the applied potentials. This is due to the fact that the amount of faradaic effect increases with the increase in the current density into the electrolyte and causes rapid increase in material dissolution rate.

Tool electrode baseline potential, the median voltage value of the waveform's flat base, also plays an important role in the determination of microhole diameter. From Fig. 10, it is observed that the MRR decreases with the increase in the baseline potential during μECM. When the

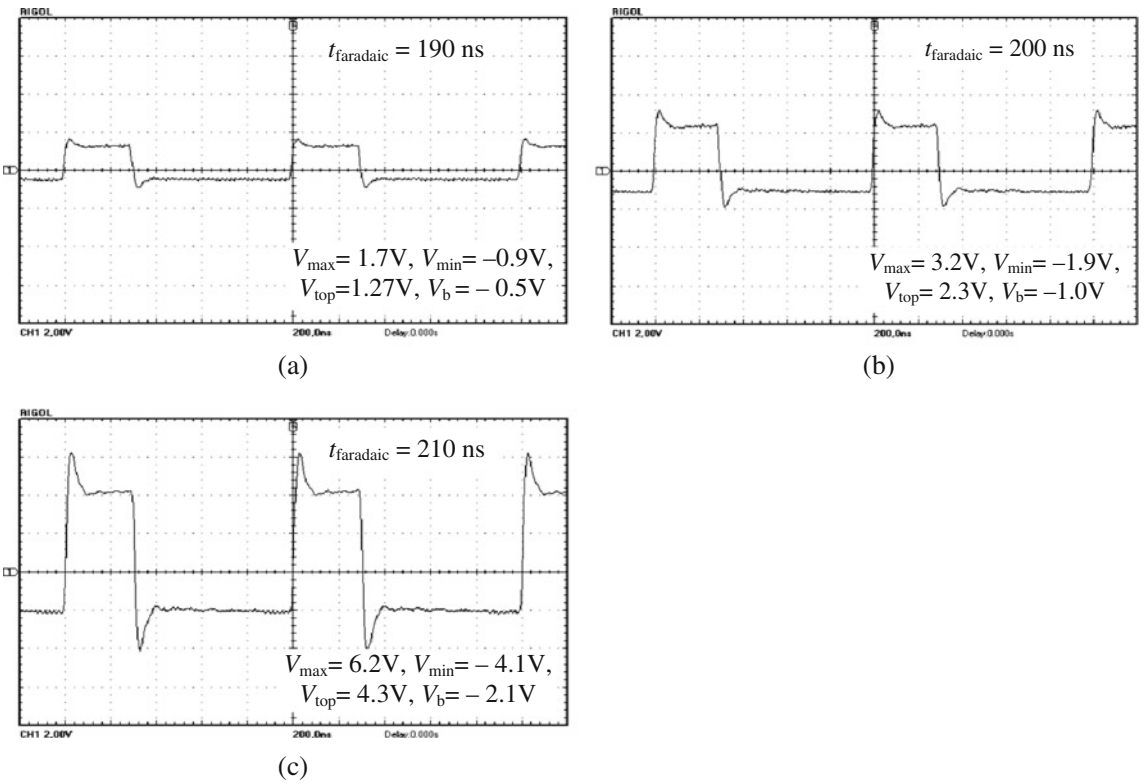

Fig. 9 Waveforms generated during machining for different peak-to-peak voltage, **a** 4.6 V, **b** 8.4 V, and **c** 17.2 V

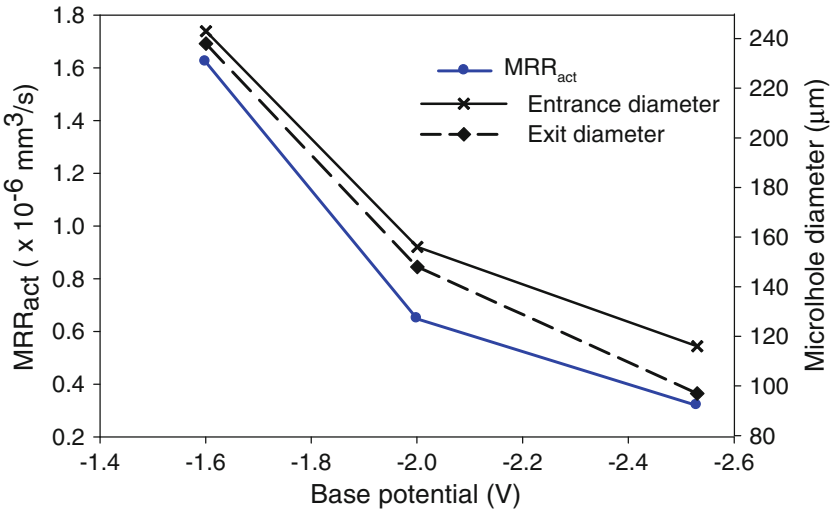

Fig. 10 Effect of baseline potential on MRR_{act} and the fabricated microholes for f=1 MHz, pulse time, τ=1.0 µs, duty cycle, δ_τ=30%, 0.2 M HCl electrolytes

baseline potential was in the range of −1.5 to −2.0 V, machining rate was quite high. Machining was possible for the baseline potential up to −2.5 V. However, after this limit, the amount of faradaic current decreased rapidly and the resulting MRR was very low. Moreover, dissolved metal was deposited on the work zone. This is because transient state enlarges with the baseline potential as shown in Fig. 11. It is observed that the amount of faradaic effect decreases and nontransient current increases with the increase in baseline potential. These nontransient currents are governing the process, resulting rapid reduction in the MRR. In the last figure (when V_b=2.18 V), the amount of nontransient current is sufficiently high; therefore, no dissolution occurs in this case. As a result, total time to remove the same volume of material increases and MRR decreases. From the results, it is recommended that the baseline potential should be in the range of −1.5 to −2.0 V for better machining as can also be found in [10].

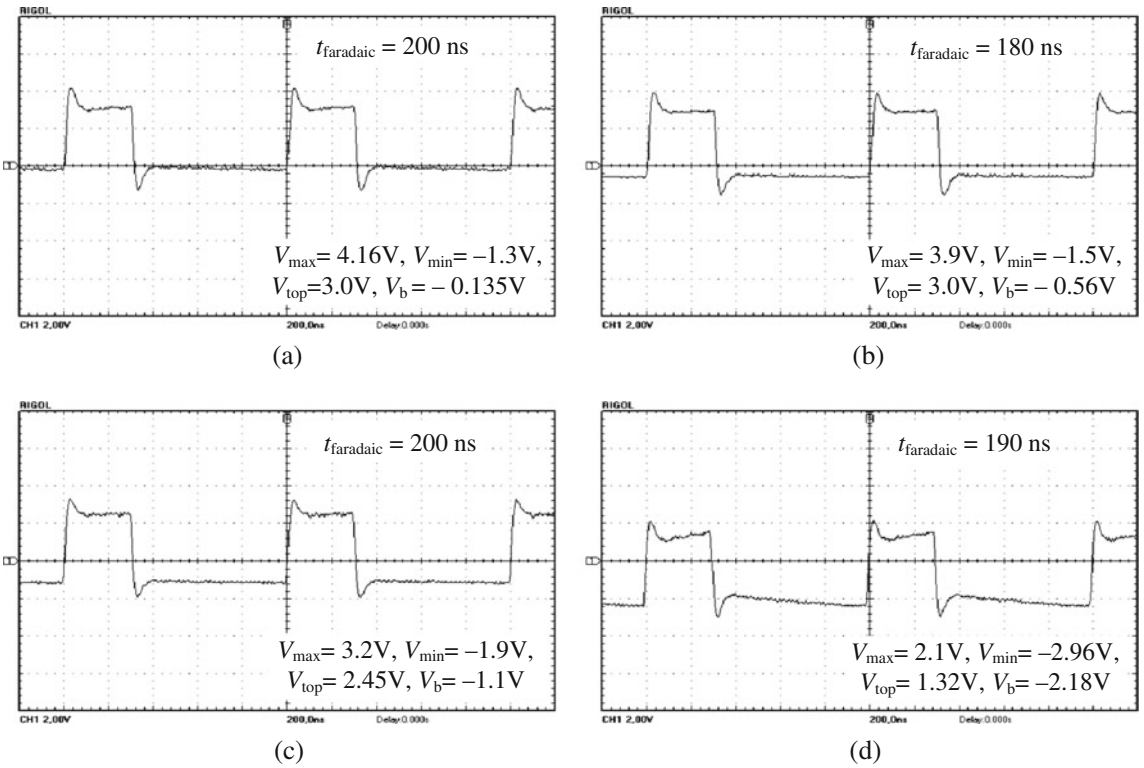

Fig. 11 Waveforms generated during machining for frequency, f=1.0 MHz, τ_p=1 µs, τ_{on}=0.3 µs, τ_{off}=0.7 µs, and peak voltage, V_{pp}=15 V, and baseline potential of **a** −1.6 V, **b** −2.0 V, **c** −2.53 V, and **d** −3.6 V

Moreover, machining was not possible for the baseline potential higher than 2.6 V. The entrance and exit diameter of the fabricated microholes are also shown in Fig. 10.

3.4 Effect of applied frequency on the waveform

A short microtool (76 μm in diameter, 690 μm in length) was selected and machining was carried out keeping all parameters fixed except applied frequency. Figure 12 exhibits the influence of frequency on waveform generated during microdrilling processes. From the figure, it is clear that the amount of faradaic current decreases with an increase in applied frequency. However, it is also observed that for the same range of pulse-on time, the amount of faradaic effect is found to be much higher for the lower applied frequency, and it decreases rapidly with the increase in applied frequency, as illustrated in Fig. 12.

From the aforementioned figure, it is observed that the voltage values acquired by the oscilloscope are not in a regular manner compared to the waveforms shown for microtool diameter effect or tool length effect. But the time for faradaic current ($t_{faradaic}$) is very high for low applied frequency and decreases rapidly with an increase in applied frequency. Therefore, the faradaic current, as well as, the total faradaic effect, decreases with applied frequency. This faradaic effect influencing on the MRR_{act}, machining time, and the dimensions of the fabricated microholes, as illustrated in Fig. 13. From the figure, it is also clear that with the increase of the faradaic current, MRR increases, machining time decreases, and microhole diameters increase with an increase in applied frequency.

3.5 Effect of duty cycle on the waveform

Together the pulse-on time (τ_{on}) and off time (τ_{off}) pulses comprise a single cycle, and duty cycle is the proportion of on time (in percentage) to the regular interval or period of time cycle. As the frequency determines the pulse period, this section describes the effect of duty cycle with applied frequency during microdrilling on nickel plate. The prefabricated short microtool (L=690 μm) was employed for this study and the machining carried out keeping the other parameters fixed. Figure 14 exhibits the influence of duty cycle on the generation of waveforms during microdrilling. With the increase in the duty cycle, both the faradaic current and the period of faradaic current are increasing, therefore, the amount of faradaic effect increases rapidly.

Figure 15 exhibits the influence of duty cycle on the amount of faradaic effect, actual material removal rate,

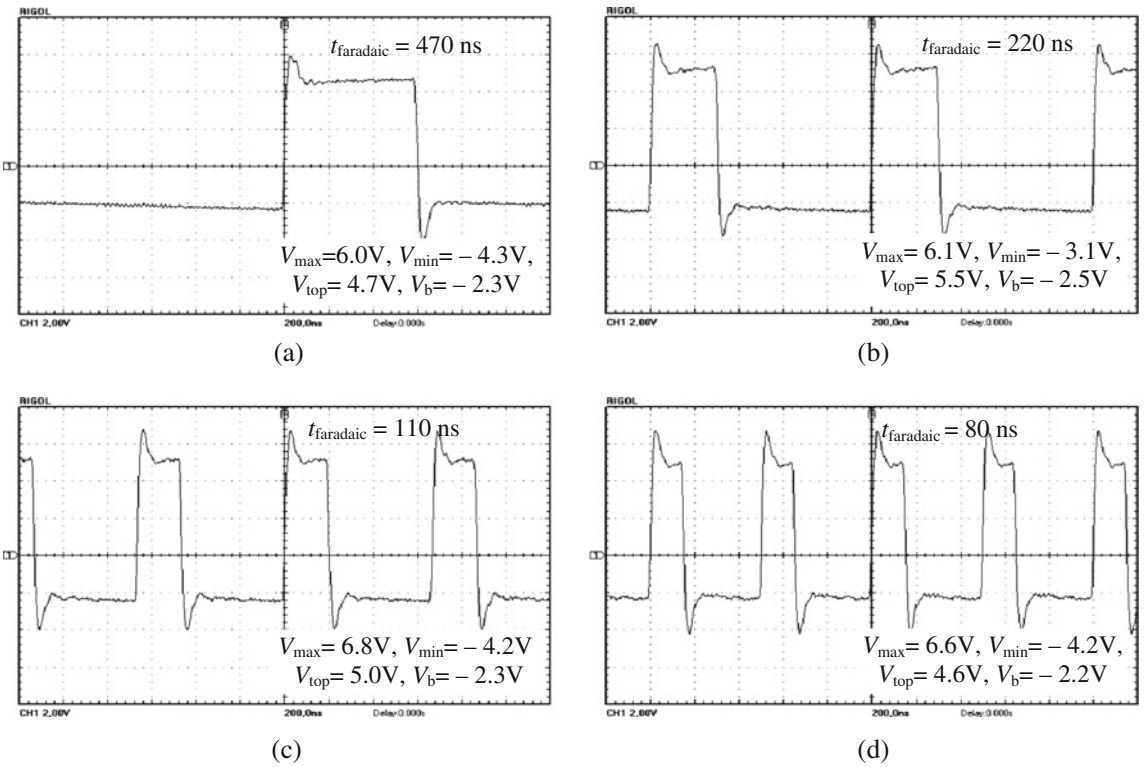

Fig. 12 Waveforms generated during machining for **a** f=0.5 MHz, τ_{on}=0.6 μs, **b** f=1 MHz, τ_{on}=0.3 μs, **c** f=1.5 MHz, τ_{on}=0.2 μs, and **d** f= 2 MHz, τ_{on}=0.15 μs, τ_{off}=0.35 μs

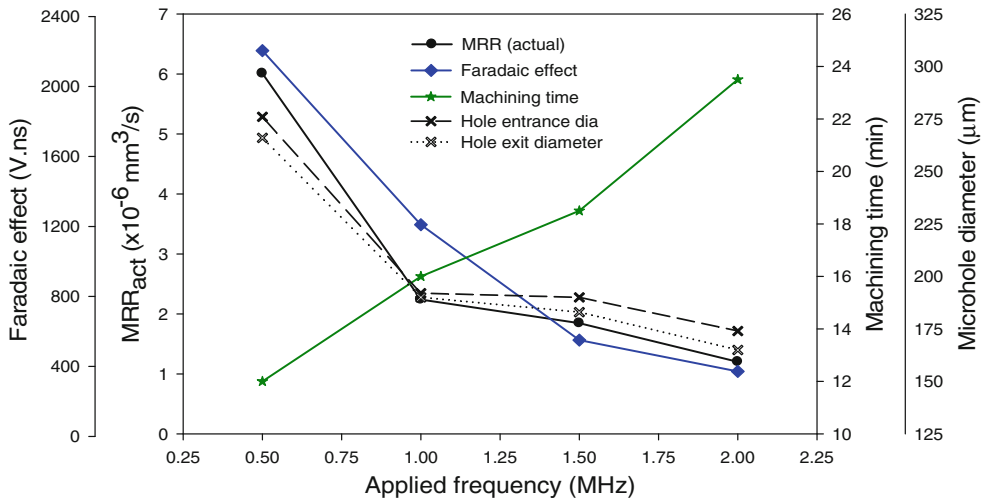

Fig. 13 Effect of applied frequency on faradaic effect, MRR_{act}, machining time, and the fabricated microholes

machining time, and the diameters of the fabricated microholes during microdrilling processes. From the figure, it is found that the amount of faradaic effect increases with the duty cycle, as a consequence, MRR_{act} and the machining time, respectively, increases and decreases with an increase in duty cycle. However, for the same applied frequency, MRR_{act} is found to be much higher for high percentage of pulse-on time. This observation can also be explained in accordance to the ion migration theory. The electrochemical machining is affected by the conductivity of the electrolyte which is primarily determined by the concentration of ions, and mobility of ions in a given electric field. During electrochemical machining, the rate of electrochemical reactions is exponentially dependent on the voltage drop in the double layer; the reaction at the workpiece is strongly confined to the charged region [12]. Hence, the mobility of ions increases with the increase of pulse-on time and smaller interelectrode gap, which ultimately increases the amount of faradaic current in the electrolyte. This increased amount of faradaic current allows not only higher material

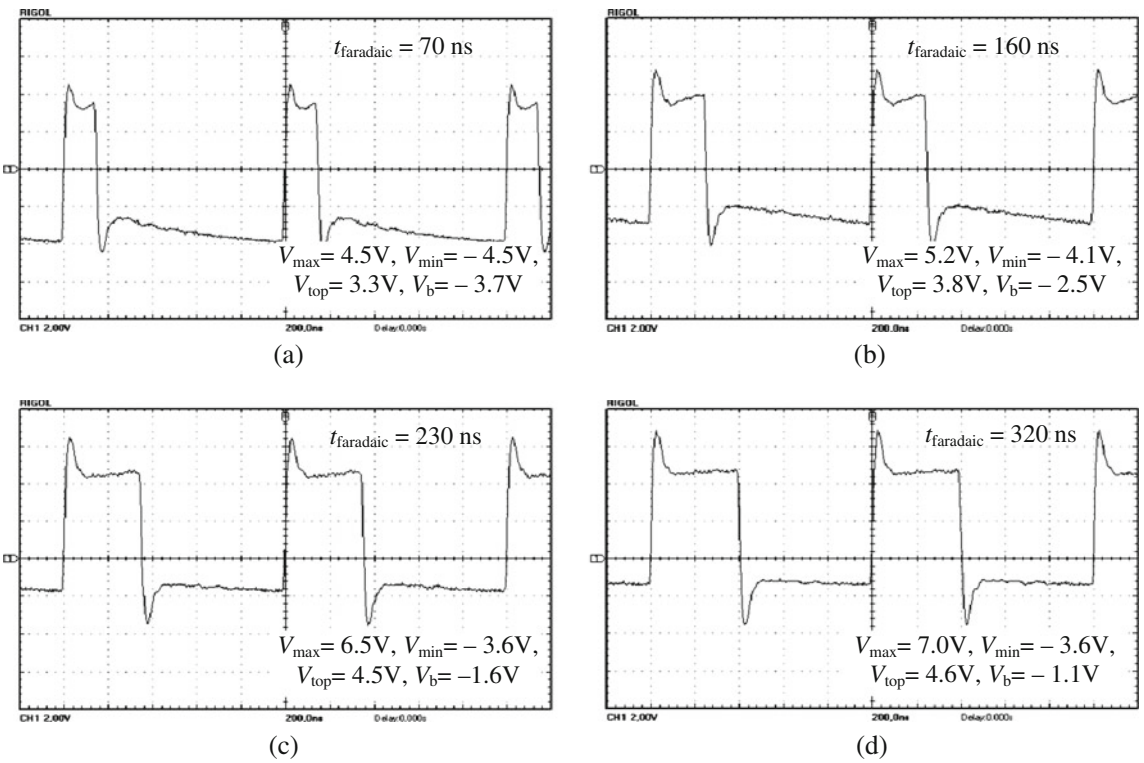

Fig. 14 Waveform generated for applied frequency, f=1 MHz, τ_p=1 μs, and duty cycle of **a** δ_τ=15%, **b** δ_τ=25%, **c** δ_τ=35%, **d** δ_τ=40%

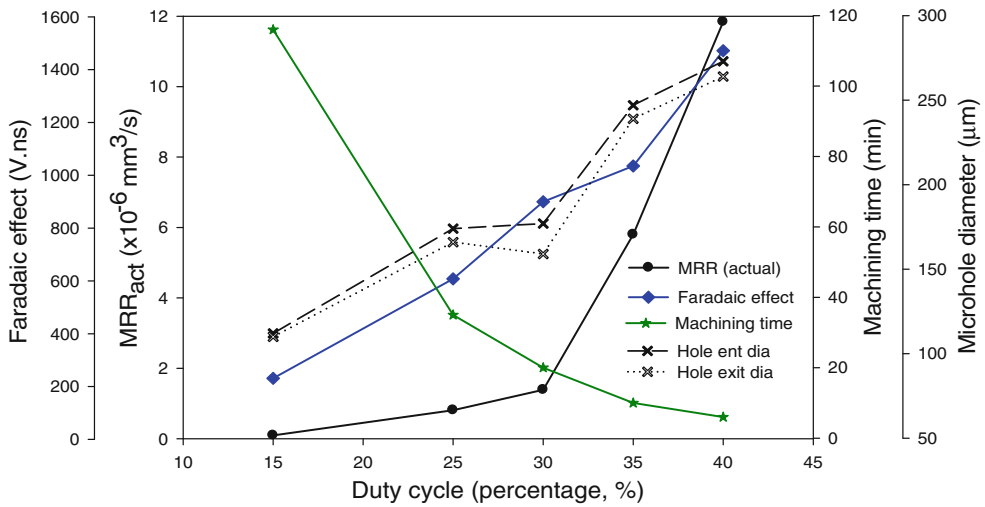

Fig. 15 Effect of duty cycle on faradaic effect, MRR_{act}, machining time, and the fabricated microholes

erosion rate, but also faster ramping up when the pulse is turned on. Therefore, the MRR_{act} increases, machining time decreases, and the dimensions of microhole size increase with duty cycles.

3.6 Effect of feed rate on the waveform

To perform micromachining effectively, microtool feed rate should have a linear relationship with the material removal rate. Therefore, the feed rate needs to be adjusted with MRR, which effects on the machining time. In this experiment, when the applied frequency was high (2 MHz), and/or duty cycle was reduced to a value less than 25%, and tailored circuit was not integrated to the feed control device, a sudden jump in the current density occurred, that could be monitored with the digital storage oscilloscope. This jumping in waveform indicates that possible corrective action is needed by holding the tool in stand-by mode until the current density drops under a certain value or stop feeding and setting a reduced value for the tool feed rate to prevent the microtool tip. The attempt has been made until a stable current density is achieved. Otherwise, the high feeding rate is very much detrimental both for microtool and the workpiece, results the distortion of the microtool tip or bending the microtools in a few micrometers range of tool length. A typical short circuit state has been recorded and the distorted microtool tip is shown in Fig. 16.

4 Conclusions

This study details the first step of the development of in-process monitoring system based on a digital data storage oscilloscope during electrochemical microdrilling. The outcomes of the process, i.e., the MRR, machining time, the dimensions of fabricated microholes, etc., are predicted from the waveform generated during machining and control action has been taken accordingly. From these experiments, it is evident that the waveform generated during machining bears significant information about the MRR, machining time, and the dimension of fabricated microholes. With the increase in microtool diameter and/or with the reduction of microtool length, the amount of faradaic current increases that eventually increases MRR. Similarly, with the increase in applied frequency or with the

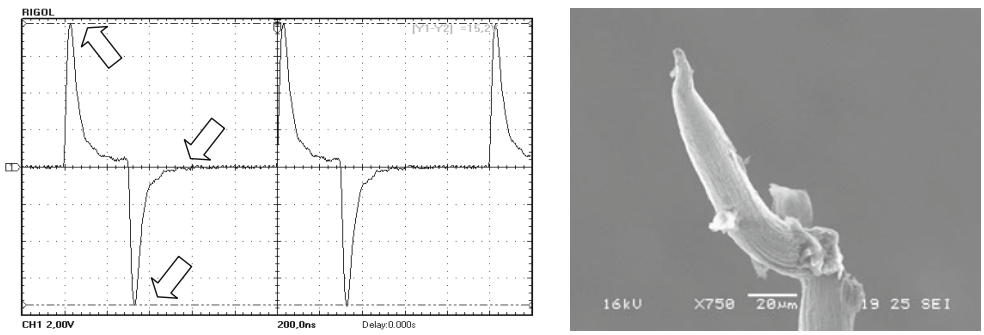

(a) (b)

Fig. 16 **a** Waveform for a typical short circuit and **b** deformed microtool tip

reduction of duty cycle, the faradaic current decreases, i.e., MRR decreases and machining time increases. A large machining time makes a microhole of large dimension but side gap ratio decreases with machining time. During machining, the short-circuit phenomenon is also frequently observed, that can be monitored and controlled.

Acknowledgment The authors acknowledge Department of Mechanical, Nuclear and Production Engineering, University of Pisa, and Ministero dell'Istruzione dell'Università e della ricerca, Programmi di ricerca cofinanziati (COFIN), Italia. Technical staffs of the DIMNP are also acknowledged.

References

1. Weng FT (2005) A study of supersonic-aided electrolysis. Int J Adv Manuf Technol 25:480–483
2. Lee ES, Shin TH, Kim BK, Baek SY (2010) Investigation of short pulse electrochemical machining for groove process on Ni-Ti shape memory alloy. Int J Prec Eng Manuf 11(1):113–118
3. Fan ZW, Hourng LW (2009) The analysis and investigation on the microelectrode fabrication by electrochemical machining. Int J Mach Tools Manuf 49:659–666
4. Bhattacharyya B, Mitra S, Boro AK (2002) Electrochemical machining: new possibilities for micromachining. Robot CIM Int Manuf 18:283–289
5. Bhattacharyya B, Malapati M, Munda J, Sarkar A (2007) Influence of tool vibration on machining performance in electrochemical micro-machining of copper. Int J Mach Tools Manuf 47 (2):335–342
6. Ahn SH, Ryu SH, Choi DK, Chu CN (2004) Electro-chemical micro drilling using ultra short pulses. Precis Eng 28:129–134
7. Lee ES, Baek SY, Cho CR (2007) A study of the characteristics for electrochemical micromachining with ultrashort voltage pulses. Int J Adv Manuf Technol 31:762–769
8. Schuster R, Kirchner V, Allongue P, Ertl G (2000) Electrochemical micromachining. Science 289(5476):98–101
9. Kock M, Kirchner V, Schuster R (2003) Electrochemical micromachining with ultrashort voltage pulses—a versatile method with lithographical precision. Electrochim Acta 48:3213–3219
10. Ryu SH (2009) Micro fabrication by electrochemical process in citric acid electrolyte. J Mater Process Technol 209:2831–2837
11. Park JW, Lee DW (2009) Pulse electrochemical polishing for microrecesses based on a coulostatic analysis. Int J Adv Manuf Technol 40:742–748
12. Wang J (2006) Analytical electrochemistry, 3rd edn. Wiley, New Jersey
13. Bard AJ, Faulkner LR (2001) Electrochemical methods: fundamentals and applications, 2nd edn. Wiley, New York
14. Park BJ, Kim BH, Chu CN (2006) The effects of tool electrode size on characteristics of micro electrochemical machining. CIRP Ann Manuf Technol 55(1):197–200
15. Mithu MAM, Fantoni G, Ciampi J (2011) The effect of high frequency and duty cycle in electrochemical microdrilling. Int J Adv Manuf Technol. doi:10.1007/s00170-010-3123-3
16. Lu Y, Liu K, Zhao D (2010) Experimental investigation on monitoring interelectrode gap of ECM with six-axis force sensor. Int J Adv Manuf Technol. doi:10.1007/s00170-010-3105-5
17. Kurita T, Chikamori K, Kubota S, Hattori M (2006) A study of three-dimensional shape machining with an ECμM system. Int J Mach Tools Manuf 46:1311–1318
18. Choi SH, Ryu SH, Choi DK, Chu CN (2007) Fabrication of WC micro-shaft by using electrochemical etching. Int J Adv Manuf Technol 31:682–687
19. Zhu D, Rajurkar KP, Wei B (1997) Modeling and monitoring and control systems. J Manuf Sci Eng Trans ASME 119(4):770–775
20. Lu YH, Zhao DB, Zhu D (2004) Mechanical property analysis of inter-electrode gap in electrochemical machining based on six force components. Chin J Mech Eng 15(23):2142–2145
21. Rivera JL, Michalek DJ, Sutherland JW (2007) Air quality in manufacturing. In: Kutz M (ed) Environmentally conscious manufacturing. Wiley, New Jersey, pp 145–178
22. Lim YM, Lim HJ, Liu JR, Kim SH (2003) Fabrication of cylindrical micropins with various diameters using DC current density control. J Mater Process Technol 141:251–255
23. De Silva AKM, McGeough JA (1998) Process monitoring of electrochemical micromachining. J Mater Process Technol 76:165–169
24. Bhattacharyya B, Munda J, Malapati M (2004) Advancement in electrochemical micro-machining. Int J Mach Tools Manuf 44:1577–1589